J Musculoskelet Neuronal Interact 2026; 26(1):147-161

Journal of Musculoskeletal and Neuronal Interactions JMNI

Original Article

METTL3-mediated GLUD1 m6A Modification Promotes Hydrogen Peroxide-induced Mitochondrial Dysfunction in Human Nucleus Pulposus Cells Via the Glutamate/α-KG Metabolic Axis

Ming Bai[1], Yimin Wu[1], Yang Zhang[1], Haibin Zhang[1], Peng Wang[1], Shuwen Li[1]

[1]Section C, Spine Surgery Center, the Second Affiliated Hospital of Inner Mongolia Medical University, China

Abstract

Objectives: Human nucleus pulposus cells (HNPCs), the primary cellular constituents of the intervertebral disc, are central to the pathogenesis of intervertebral disc degeneration (IVDD). Oxidative stress–induced mitochondrial dysfunction leads to intracellular metabolic imbalance and has been implicated in IVDD. This study investigated the role and molecular mechanism of glutamate dehydrogenase 1 (GLUD1) in hydrogen peroxide (H_2O_2)–challenged HNPCs relevant to IVDD. **Methods:** HNPCs were exposed to H_2O_2 to establish an oxidative stress model. Cell viability was assessed using the CCK-8 assay. Mitochondrial function was evaluated by measuring the oxygen consumption rate (OCR) and mitochondrial membrane potential. GLUD1 expression was quantified by qRT-PCR and Western blotting. The regulatory relationship between METTL3 and GLUD1 was examined by MeRIP-qPCR and a luciferase reporter assay. **Results:** H_2O_2 treatment decreased OCR and mitochondrial membrane potential in HNPCs and reduced alpha-ketoglutarate (α-KG) levels and GLUD1 expression. GLUD1 knockdown exacerbated H_2O_2-induced mitochondrial dysfunction, whereas GLUD1 overexpression alleviated it. METTL3 regulated GLUD1 mRNA stability by inducing GLUD1 m6A modification via YTHDF2, thereby modulating H_2O_2-induced mitochondrial dysfunction. **Conclusion:** GLUD1 protects HNPCs from H_2O_2-induced mitochondrial dysfunction through the glutamate/α-KG metabolic axis.

Keywords: Human Nucleus Pulposus Cells, Intervertebral Disc Degeneration, GLUD1, Glutamate/α-KG axis, Mitochondrial Dysfunction

Introduction

Intervertebral disc degeneration (IVDD) is a leading cause of chronic low back pain and has a high incidence and disability burden among middle-aged and older adults[1]. Recently, artificial intelligence has shown high accuracy, sensitivity, and specificity for detecting and grading IVDD using the Pfirrmann system[2,3]. Current treatments primarily relieve symptoms rather than target the underlying pathology[4]. Therefore, elucidating the molecular mechanisms of IVDD may facilitate the development of new therapeutic approaches.

The nucleus pulposus (NP) is a principal component of the intervertebral disc (IVD)[5]. Human nucleus pulposus cells (HNPCs) are among the first to exhibit degenerative changes during IVDD and are crucial in disease progression[6]. By regulating extracellular matrix homeostasis, HNPCs maintain the normal structure and function of the IVD[7]. Consequently, increasing attention has been directed toward preserving HNPC homeostasis as a potential therapeutic strategy for IVDD[8].

The hypoxic IVD microenvironment fosters oxidative stress and mitochondrial metabolic abnormalities[9]. ROS, key intermediary metabolites, have been implicated in the

The authors have no conflict of interest.

Corresponding author: Shuwen Li, Section C, Spine Surgery Center, the Second Affiliated Hospital of Inner Mongolia Medical University, No. 59, Korqin Expressway Road, Saihan District, Hohhot 10030, China
E-mail: nmgykdxefy@163.com

Edited by: G. Lyritis
Accepted 15 December 2025

pathogenesis of IVDD[10]. Under various pathological stimuli, ROS production in HNPCs increases markedly[11]. When ROS levels exceed physiological thresholds, NP cells develop mitochondrial dysfunction and metabolic imbalance[12]. ROS-induced mitochondrial dysfunction, in turn, amplifies ROS generation through a positive feedback loop, leading to sustained oxidative damage[13]. Restoring mitochondrial function may counteract oxidative stress and subsequent cell death, thereby delaying IVD degeneration[14]. Thus, deeper insight into the metabolic mechanisms of, and interventions for, mitochondrial dysfunction could inform the pathogenesis and treatment of IVDD.

The identification of biomarkers associated with mitochondrial metabolism has significant clinical relevance. Employing machine-learning algorithms, such as artificial neural networks, facilitates biomarker screening and selection[15]. These biomarkers can serve as valuable clinical tools for early diagnosis, risk stratification, and prediction of therapeutic responses, ultimately enhancing personalized treatment strategies for individuals with IVDD[16].

Glutamate dehydrogenase 1 (GLUD1) is an evolutionarily conserved mitochondrial enzyme that regulates glutamate metabolism[17]. GLUD1 is mainly located in the mitochondrial matrix but is also present in the cytoplasm and endoplasmic reticulum[18]. This intracellular distribution underlies its regulatory role in mitochondrial metabolism and redox homeostasis[19]. GLUD1 catalyzes the reversible oxidative deamination of L-glutamate to α-KG, a tricarboxylic acid (TCA) cycle intermediate, thereby contributing to recycling amino acids into the TCA cycle to support mitochondrial energy production[20]. α-KG provides nitrogen and carbon skeletons for the synthesis of amino acids, nucleotides, and lipids[21]. GLUD1 activity is tuned to cellular energy requirements, being negatively regulated by GTP and positively regulated by ADP[22]. Previous studies on GLUD1 have largely focused on neuropsychiatric disorders and cancer (e.g., schizophrenia, major depressive disorder, hepatocellular carcinoma)[18,23]. One mechanism by which GLUD1 acts in disease is through regulation of glutamine metabolism[24]. Here, we investigated the potential role of GLUD1 in IVDD.

N-6-methyladenosine (m6A) is an epitranscriptomic RNA modification that regulates gene expression by influencing RNA translation, stability, and other processes[25]. Studies have shown that the progression of IVDD is regulated by m6A methylation[26]. The m6A pathway involves three classes of proteins: m6A methyltransferases ("writers"), m6A demethylases ("erasers"), and m6A recognition factors ("readers")[27]. m6A is installed by writers, which form methyltransferase complexes that add a methyl group to the N6 position of adenine within specific sequence motifs, while demethylases reverse this modification[26]. The overall level of m6A is determined by the balanced activity and expression of writers and erasers[28]. YTH-domain family proteins are specific m6A readers that regulate mRNA degradation. For example, YTHDF2 recognizes m6A-modified transcripts through its C-terminal YTH domain and promotes their decay[29]. Thus, transcripts execute corresponding regulatory outcomes through recognition by readers[30]. Given this evidence, m6A methylation may participate in the epigenetic regulation of IVDD.

In this study, H_2O_2 exposure reduced the oxygen consumption rate (OCR) and mitochondrial membrane potential in HNPCs and decreased α-KG levels and GLUD1 expression. GLUD1 alleviated H_2O_2-induced mitochondrial dysfunction. We hypothesized that methyltransferase-like 3 (METTL3) regulates GLUD1 expression by installing GLUD1 m6A modifications that are recognized by YTHDF2. Thus, GLUD1 protects HNPCs from H_2O_2-induced mitochondrial dysfunction via the glutamate/α-KG axis. These findings provide new insight into mitochondrial metabolism in HNPCs and suggest a potential therapeutic strategy for IVDD.

Materials and Methods

Cell culture and treatment

Human nucleus pulposus cells (HNPCs; HUM-iCell-s012) were purchased from iCell Bioscience (Shanghai, China) and cultured in DMEM (D6046; Sigma-Aldrich, St. Louis, MO, USA) supplemented with 10% FBS and 1% penicillin/streptomycin. Cultures were maintained at 37°C in 5% CO_2. The cell line was authenticated by STR profiling. One week before experiments, cultures were confirmed to be free of mycoplasma contamination by PCR. HNPCs were treated for 24 h with H_2O_2 (0, 50, 100, or 200 μM) in the absence or presence of the METTL3 inhibitor STM2457 (5 μM; S9870; Selleck, Shanghai, China) or 0.01% (v/v) DMSO vehicle. STM2457 was prepared as a 10 mM stock in DMSO; the final DMSO concentration in all groups (including untreated and H_2O_2-only) was matched to 0.01% (v/v) by back-filling with DMSO.

Knockdown and overexpression

Sequences of small interfering RNAs (siRNAs) targeting GLUD1 and YTHDF2 are as follows: siGLUD1-1, GAACUAUACUGAUAAUGAAUU; siGLUD1-2, GAAGAUCUAUGGUUGACUAAU; siGLUD1-3, AGAUCUUCC UGGAGAGAAACA; siYTHDF2-1, GCACAGAAGUUGCAAGC AAUG; and siYTHDF2-2, GGAGAAUAUAACAGUGUUACC. HNPCs were transfected for 4–6 h with siRNA or a pcDNA3.1 expression plasmid using Lipofectamine. Scramble siRNA (siNC) and a blank pcDNA3.1 plasmid (oeNC) served as negative controls.

Cell viability

Cell viability was assessed using Cell Counting Kit-8 (CCK-8; C0039; Beyotime Biotechnology, Shanghai, China). HNPCs were seeded into 96-well plates and incubated overnight. 10 μL of CCK-8 reagent were added to each well, and absorbance at 450 nm was measured with a microplate reader (BioTek, San Jose, CA, USA).

Flow cytometry

Mitochondrial membrane potential (MMP) was assessed using a JC-1 assay kit (C2006; Beyotime Biotechnology). HNPCs (0.5 mL at 5×10^5 cells/mL) were mixed with an equal volume of JC-1 staining solution and incubated. Cells were washed twice with JC-1 staining buffer, resuspended, and analyzed by flow cytometry (BD Biosciences, San Jose, CA, USA). ΔΨm was quantified as the red (aggregate)/green (monomer) fluorescence ratio, where red aggregates indicate polarized mitochondria and green monomers indicate depolarization. Representative flow-cytometry plots (gating strategy, compensation, positive/negative controls) are shown in Supplementary Figure S1.

Extracellular flux analysis

OCR was measured using a Seahorse XF Cell Mito Stress Test Kit (103015-100; Seahorse Bioscience, North Billerica, MA, USA) on a Seahorse XFe96 Extracellular Flux Analyzer, following the manufacturer's instructions. HNPCs were seeded in XFe96/XF Pro cell culture microplates (103794-100; Seahorse Bioscience) at 1×10^5 cells/well and cultured overnight for attachment. Before the assay, Seahorse XF calibration solution was added to a utility plate fitted with a Hydro Booster and sensor cartridge, then placed overnight in a 37°C, CO_2-free incubator with a hydration probe. The assay medium was prepared with DMEM supplemented with 10 mM glucose, 2 mM glutamine, and 1 mM pyruvate. Cells were washed twice with assay medium and incubated for 1 h at 37°C in a CO_2-free incubator. Subsequently, 20 μL of 15 μM oligomycin (final concentration, 1.5 μM) was loaded into port A; 22 μL of 10 μM FCCP (final concentration, 1 μM) into port B; and 25 μL of 5 μM antimycin A/rotenone (final concentration, 0.5 μM) into port C (mix time, 3 min; wait time, 2 min). OCR was normalized to cell number. Wave Controller software (version 2.6; Seahorse Bioscience) was used for data acquisition, analysis, and baseline correction.

Measurement of glutamate, alpha-ketoglutarate (α-KG), and adenosine triphosphate (ATP)

Glutamate, α-KG, and ATP were quantified using a glutamate assay kit (ab83389), an alpha-ketoglutarate assay kit (ab83431), and an ATP assay kit (ab83355) (all from Abcam, Waltham, MA, USA) according to the manufacturer's instructions.

Quantitative real-time polymerase chain reaction (qRT-PCR)

Total RNA was extracted using TRIzol reagent. The PrimeScript™ kit (6210A; Takara Biotechnology Co., Ltd.) was used to reverse transcribe RNA into cDNA. Target gene expression was quantified on an Applied Biosystems 7500 Real-Time PCR System using SYBR Green Master Mix (11203ES03; Yeasen Biotechnology, Shanghai, China). Primer sequences were as follows: GLUD1, 5′-AGGGCTTTATTGGTCCTGGC-3′ (forward) and 5′-TGCTGGCATAGGTATCAGCG-3′(reverse); GLUD2, 5′-GCGGCCAACCACTCGG-3′(forward) and 5′-CACCAACTTGTCCTCCACGA-3′(reverse); YTHDF2, 5′-GGCAGTGGGTTCGGTCATAA-3′ (forward) and 5′-GGACCGAAGCTTCTCCAACA-3′ (reverse); ACTB, 5′-CCGCGAGAAGATGACCCAG-3′ (forward) and 5′-GATAGCACAGCCTGGATAGCA-3′ (reverse). ACTB served as the endogenous reference. Relative mRNA levels were calculated using the $2^{-\Delta\Delta Ct}$ method.

Western blot

Cell proteins were separated by electrophoresis and transferred to PVDF membranes. Membranes were blocked in 5% nonfat milk for 2 h and then incubated overnight with primary antibodies against GLUD1 (ab153973; Abcam), GLUD2 (PA5-112429; Invitrogen, Carlsbad, CA, USA), YTHDF2 (ab220163; Abcam), and β-actin (66009-1-Ig; Proteintech Group, Inc., Rosemont, IL, USA). Subsequently, membranes were incubated with secondary antibodies (ZB-2301, ZB-2305; ZSGB-BIO, Beijing, China). Protein bands were visualized using an enhanced chemiluminescence detection kit (WBKLS0100; Millipore, Burlington, MA, USA). Uncropped Western blots with molecular weight markers for all quantified bands are shown in Supplementary Figure S2.

Luciferase reporter assay

Cells treated with 100 μM H_2O_2, with or without STM2457, were transfected with the pGL3–GLUD1 3′-UTR luciferase reporter plasmid and the pRL-TK vector expressing Renilla luciferase using Lipofectamine 2000 (Invitrogen). The Dual-Luciferase Reporter Assay System (E1910; Promega Corporation, Madison, WI, USA) was used to measure relative luciferase activity 48 h after transfection.

mRNA stability

Cells were treated with 100 μM H_2O_2, with or without STM2457, and then actinomycin D (2 μM; S8964; Selleck) was added to block transcription. RNA was harvested at the indicated times to determine GLUD1 half-life. Total RNA from HNPCs was extracted, cDNA was synthesized by reverse transcription, and mRNA levels were quantified by qRT-PCR.

RNA immunoprecipitation (RIP) assay

RIP was performed using the Magna RIP RNA-binding protein immunoprecipitation kit (17-10499; Millipore). Cells were lysed in RIP lysis buffer, and lysates were incubated with anti-m6A (ab208577), anti-YTHDF2 (ab246514), or anti-IgG (ab172730) antibodies (all from Abcam). RNA–protein complexes were washed with RIP wash buffer, RNA was purified using phenol: chloroform: isoamyl alcohol, and target gene levels were determined by qRT-PCR.

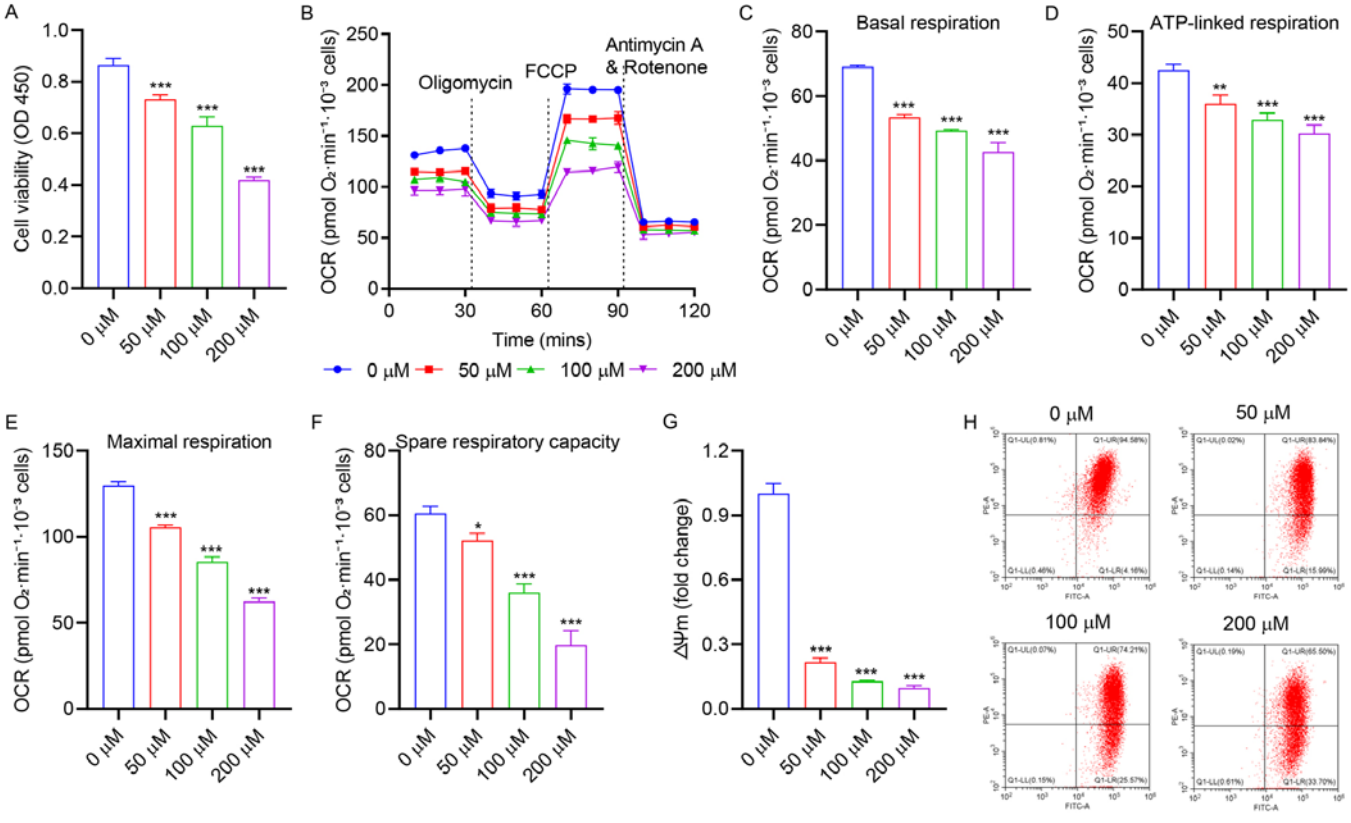

Figure 1. H_2O_2 treatment inhibits cell viability, oxygen consumption rate (OCR) and MMP in HNPCs. HNPCs were treated with different concentrations of H_2O_2 for 24 h. (A) Cell viability was detected by CCK8. (B-F) OCR was detected by XFe96 Extracellular Flux Analyzer. OCR reported as pmol $O_2 \cdot min^{-1} \cdot 10^{-3}$ cells (normalized to cell number). (G, H) MMP was detected by flow cytometry. Data are mean ± SD (n = 3 biological replicates). One-way ANOVA followed by Tukey's post hoc test was used. *p<0.05, **p<0.01, ***p<0.001 vs 0 μM.

Statistical Analysis

Data were analyzed and graphed using GraphPad Prism 8.4.2. Data are presented as mean ± standard deviation (SD). Each biological replicate represents an independent experiment; technical wells were averaged within each replicate. Group comparisons used two-sided, unpaired Student's t-tests (two groups) or one-way analysis of variance (ANOVA) with Tukey's post hoc test (≥3 groups), as appropriate. Statistical significance was set at $p < 0.05$.

Results

Effects of H_2O_2 on HNPC viability and mitochondrial function

HNPCs were treated with increasing concentrations of H_2O_2 for 24 h. Cell viability decreased significantly with higher H_2O_2 concentrations (Figure 1A). To assess mitochondrial function, we measured cellular OCR and MMP. With increasing H_2O_2, OCR—encompassing basal, ATP-linked, maximal respiration, and spare respiratory capacity—declined significantly (Figure 1B–F), as did MMP (Figure 1G,H). These data suggested that H_2O_2 effectively induces mitochondrial damage in HNPCs.

H_2O_2 inhibits α-KG production and GLUD1 expression in HNPCs

To evaluate the effect of H_2O_2 on glutamine metabolism in HNPCs, we measured intracellular glutamate, α-KG, and ATP, as well as GLUD1 and GLUD2 expression. Glutamate, α-KG, and ATP levels decreased significantly with increasing H_2O_2 concentration in a dose-dependent manner (Figure 2A–C). We then assessed GLUD1 and GLUD2. GLUD1 levels declined with higher H_2O_2 concentrations, whereas GLUD2 showed no significant change (Figure 2D,E).

Knockdown of GLUD1 exacerbates H_2O_2-induced mitochondrial dysfunction

To assess the effect of GLUD1 on mitochondrial function, GLUD1 was knocked down prior to H_2O_2 treatment

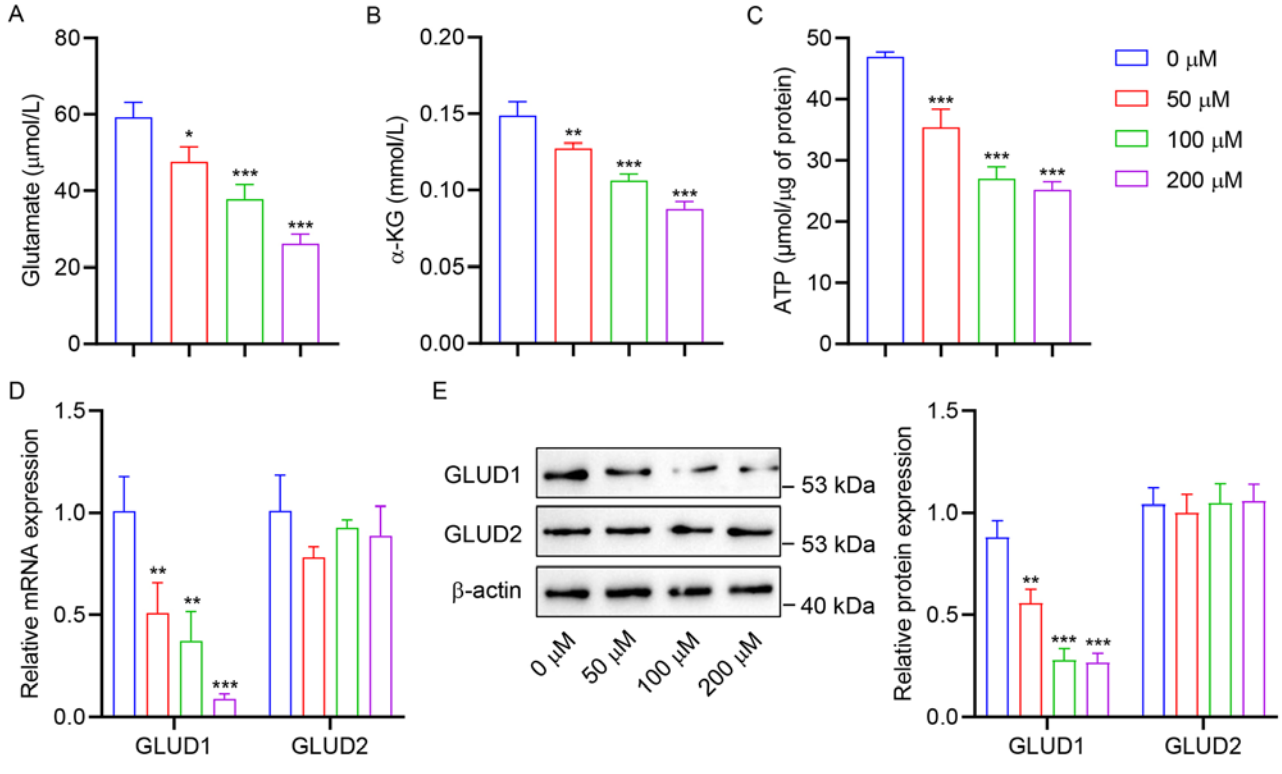

Figure 2. H_2O_2 treatment inhibits α-KG production and GLUD1 expression in HNPCs. After 24 h treatment with different concentrations of H_2O_2, the contents of (A) glutamate, (B) α-KG, (C) ATP in HNPCs were detected. The expressions of GLUD1 and GLUD2 were detected by (D) qRT-PCR and (E) Western blot. Data are mean ± SD (n = 3 biological replicates). One-way ANOVA followed by Tukey's post hoc test was used. *p<0.05, **p<0.01, ***p<0.001 vs 0 μM.

(Supplementary Figure S3A,B). Given the mitochondrial and cellular damage induced by H_2O_2 in HNPCs, we evaluated cell viability, OCR, and MMP. GLUD1 knockdown significantly reduced cell viability compared with the H_2O_2+siNC group (Figure 3A). H_2O_2 decreased OCR—including basal, ATP-linked, maximal respiration, and spare respiratory capacity—and reduced MMP; GLUD1 knockdown further decreased OCR and MMP, exacerbating mitochondrial dysfunction (Figure 3B–H). Relative to H_2O_2+siNC, GLUD1 knockdown also significantly lowered α-KG and ATP levels (Figure 3I,J). Western blotting confirmed effective GLUD1 knockdown in the siGLUD1 group (Figure 3K).

Overexpression of GLUD1 alleviates H_2O_2-induced mitochondrial dysfunction

We next examined the effect of GLUD1 overexpression on H_2O_2-induced mitochondrial dysfunction (Supplementary Figure S3C,D). Compared with the H_2O_2+oeNC group, GLUD1 overexpression significantly increased the viability of H_2O_2-treated HNPCs (Figure 4A). Relative to H_2O_2+oeNC, GLUD1 overexpression also increased OCR—including basal, ATP-linked, maximal respiration, and spare respiratory capacity—and elevated MMP, thereby mitigating the decreases caused by H_2O_2 (Figure 4B–H). In terms of glutamine metabolism, GLUD1 overexpression significantly increased α-KG and ATP levels in HNPCs (Figure 4I,J). Western blotting confirmed effective GLUD1 overexpression, with a marked increase in GLUD1 protein (Figure 4K).

METTL3 induces GLUD1 m6A modification via YTHDF2 to regulate GLUD1 mRNA stability

To determine whether m6A modification is involved in GLUD1 expression, we performed methylated RNA immunoprecipitation–qPCR (MeRIP-qPCR). Compared with IgG, m6A-specific antibodies significantly enriched GLUD1 mRNA, and inhibition of METTL3 with STM2457 markedly reduced m6A-modified GLUD1 mRNA (Figure 5A). In parallel, METTL3 inhibition increased GLUD1 3′-UTR luciferase activity (Figure 5B) and upregulated GLUD1 mRNA and protein levels (Figure 5C,D). To test whether m6A affects GLUD1 mRNA stability, cells were treated with

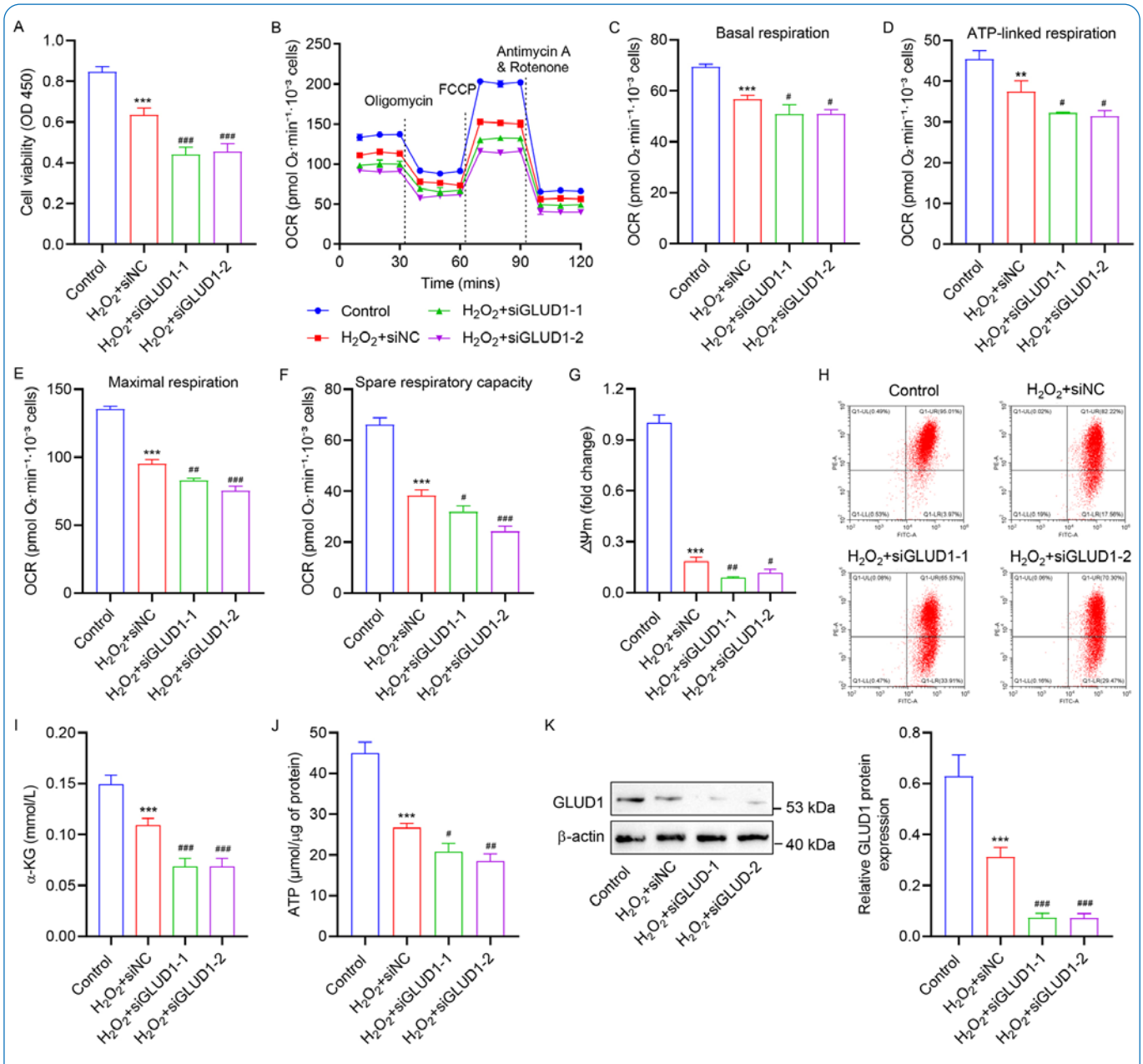

Figure 3. Knockdown of GLUD1 exacerbates H_2O_2-induced mitochondrial dysfunction in HNPCs. GLUD1 gene interfering siRNA was pre-transfected into HNPCs for 24 h, and then treated with H_2O_2 (100 μM) for 24 h. (A) Cell viability was detected by CCK8. (B-F) OCR was detected by XFe96 Extracellular Flux Analyzer. OCR reported as pmol $O_2 \cdot min^{-1} \cdot 10^{-3}$ cells (normalized to cell number). (G, H) MMP was detected by flow cytometry. (I) α-KG and (J) ATP content was analyzed by biochemical detection. (K) Western blot analysis of GLUD1 expression. Data are mean ± SD (n = 3 biological replicates). One-way ANOVA followed by Tukey's post hoc test was used. $^{**}p<0.01$, $^{***}p<0.001$ vs control. $^{\#}p<0.05$, $^{\#\#}p<0.01$, $^{\#\#\#}p<0.001$ vs H_2O_2+siNC.

the RNA polymerase II inhibitor actinomycin D. Relative to H_2O_2 alone, METTL3 inhibition increased the GLUD1 mRNA half-life and reduced its degradation (Figure 5E), indicating that METTL3 regulates GLUD1 by modulating mRNA stability. To examine the role of readers, HNPCs were transfected with YTHDF2 siRNA (Supplementary Figure S3E,F). YTHDF2 knockdown significantly increased GLUD1 levels (Figure 5F,G), and GLUD1 3′-UTR was significantly enriched by YTHDF2-specific antibodies compared with IgG (Figure 5H). Collectively, these results show that METTL3 regulates GLUD1 expression in an m6A–YTHDF2–dependent manner.

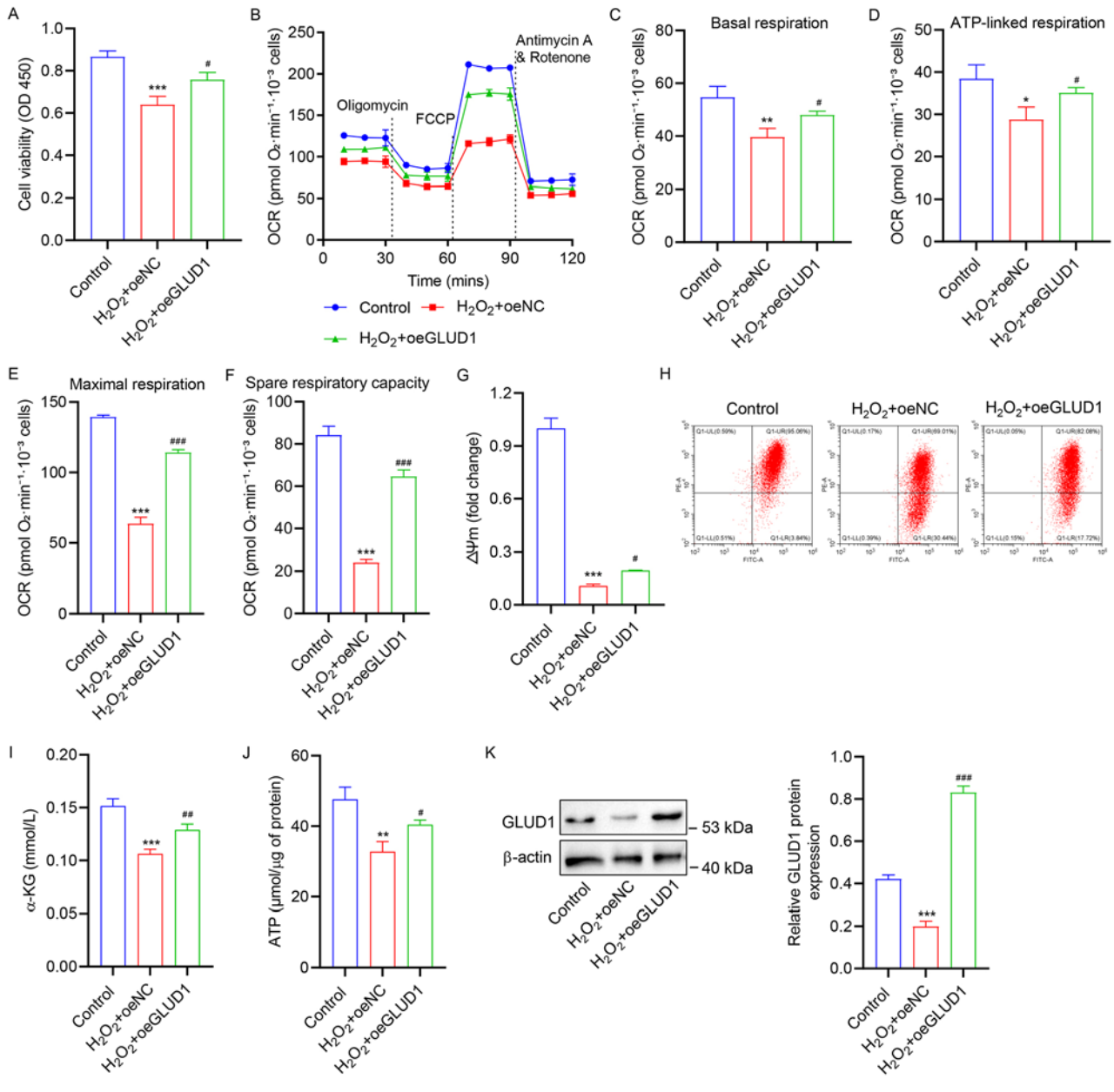

Figure 4. Overexpression of GLUD1 alleviates H_2O_2-induced mitochondrial dysfunction in HNPCs. GLUD1 overexpression vector was pre-transfected into HNPCs cells for 24 h, and then treated with H_2O_2 (100 μM) for 24 h. (A) Cell viability was detected by CCK8, (B-F) OCR was detected by XFe96 Extracellular Flux Analyzer. OCR reported as pmol $O_2 \cdot min^{-1} \cdot 10^{-3}$ cells (normalized to cell number). (G, H) MMP was detected by flow cytometry, and biochemical detection was performed for (I) α-KG and (J) ATP content. (K) Western blot detection of GLUD1 expression. Data are mean ± SD (n = 3 biological replicates). One-way ANOVA followed by Tukey's post hoc test was used. *p<0.05, **p<0.01, ***p<0.001 vs control. #p<0.05, ##p<0.01, ###p<0.001 vs H_2O_2+oeNC.

GLUD1 m6A modification induced by METTL3 regulates H_2O_2-induced mitochondrial dysfunction

To test whether METTL3-induced GLUD1 m6A modification contributes to H_2O_2-induced mitochondrial dysfunction, cells were treated with the METTL3 inhibitor STM2457 and/or GLUD1 siRNA. Compared with the H_2O_2 group, STM2457 significantly increased HNPC viability, whereas GLUD1 knockdown reversed this effect (Figure 6A). OCR analyses showed that STM2457 increased basal, ATP-linked, and maximal respiration and spare respiratory capacity, and also elevated MMP in HNPCs; GLUD1 knockdown reduced OCR and MMP, partially

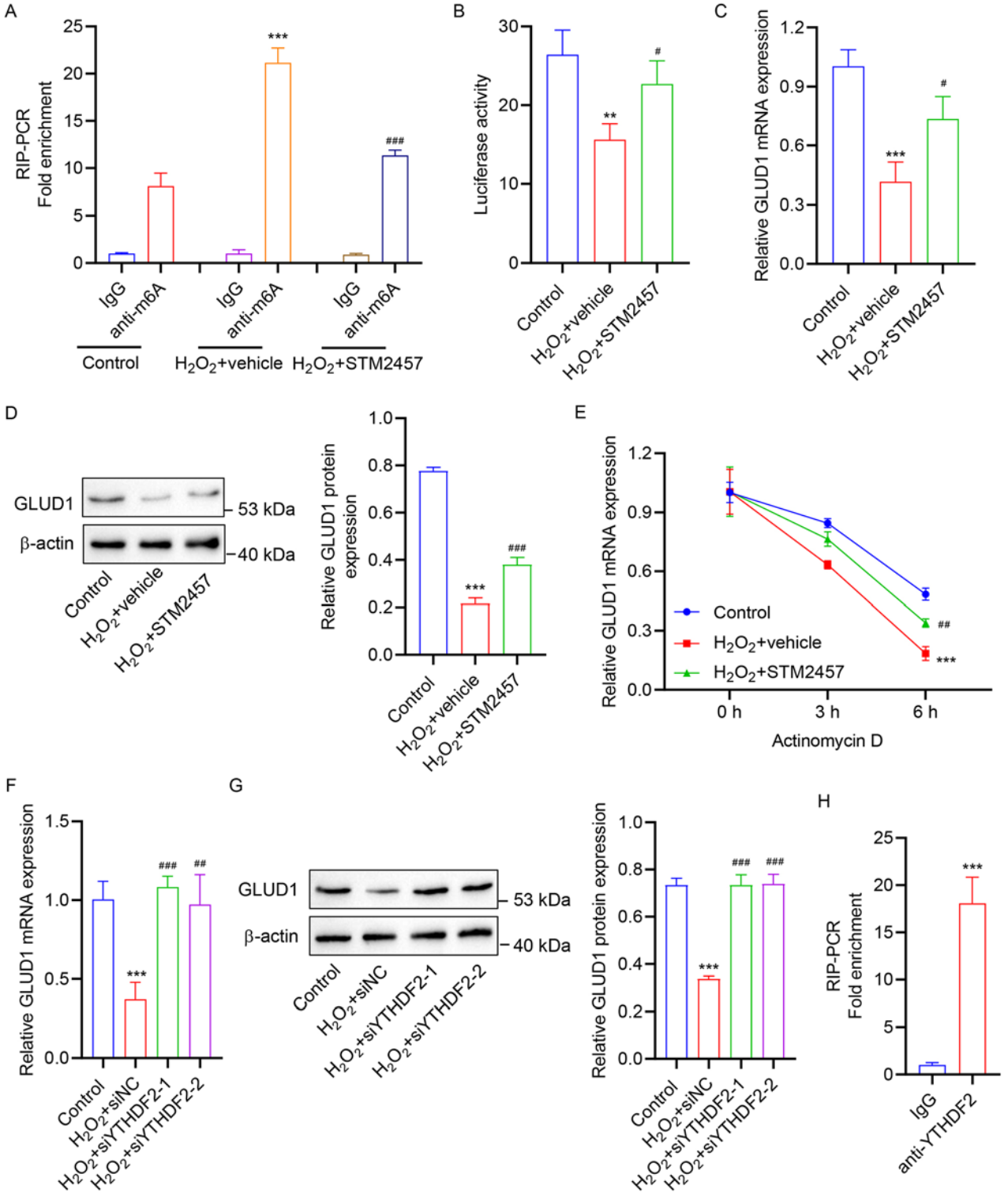

Figure 5. METTL3 induces GLUD1 m6A modification and inhibits GLUD1 mRNA stabilization via YTHDF2. HNPCs were treated with H_2O_2 (100 μM) alone or in combination with 5 μM METTL3 inhibitor STM2457 or DMSO vehicle for 24 h. All groups were DMSO-matched to 0.01% (v/v). GLUD1 3'-UTR methylation level was detected by (A) MeRIP-qPCR. GLUD1 3'-UTR activity was detected by (B) luciferase reporter gene. (C) qRT-PCR and (D) Western blot were used to detect GLUD1 expression. (E) GLUD1 expression was detected by qRT-PCR after 0 h, 3 h, and 6 h treatment with 2 μM actinomycin D. HNPCs cells were pre-transfected with YTHDF2 interfered siRNA for 24 h, and then treated with H_2O_2 (100 μM) for 24 h. (F) qRT-PCR and (G) Western blot were used to detect the expression of GLUD1. (H) RIP-qPCR was used to detect the binding of YTHDF2 to GLUD1 3'-UTR. Data are mean ± SD (n = 3 biological replicates). (A-G) One-way ANOVA followed by Tukey's post hoc test and (H) two-sided unpaired Student's t-test were used. **p<0.01, ***p<0.001 vs control or IgG. $^{\#}p$<0.05, $^{\#\#}p$<0.01, $^{\#\#\#}p$<0.001 vs H_2O_2+vehicle or H_2O_2+siNC.

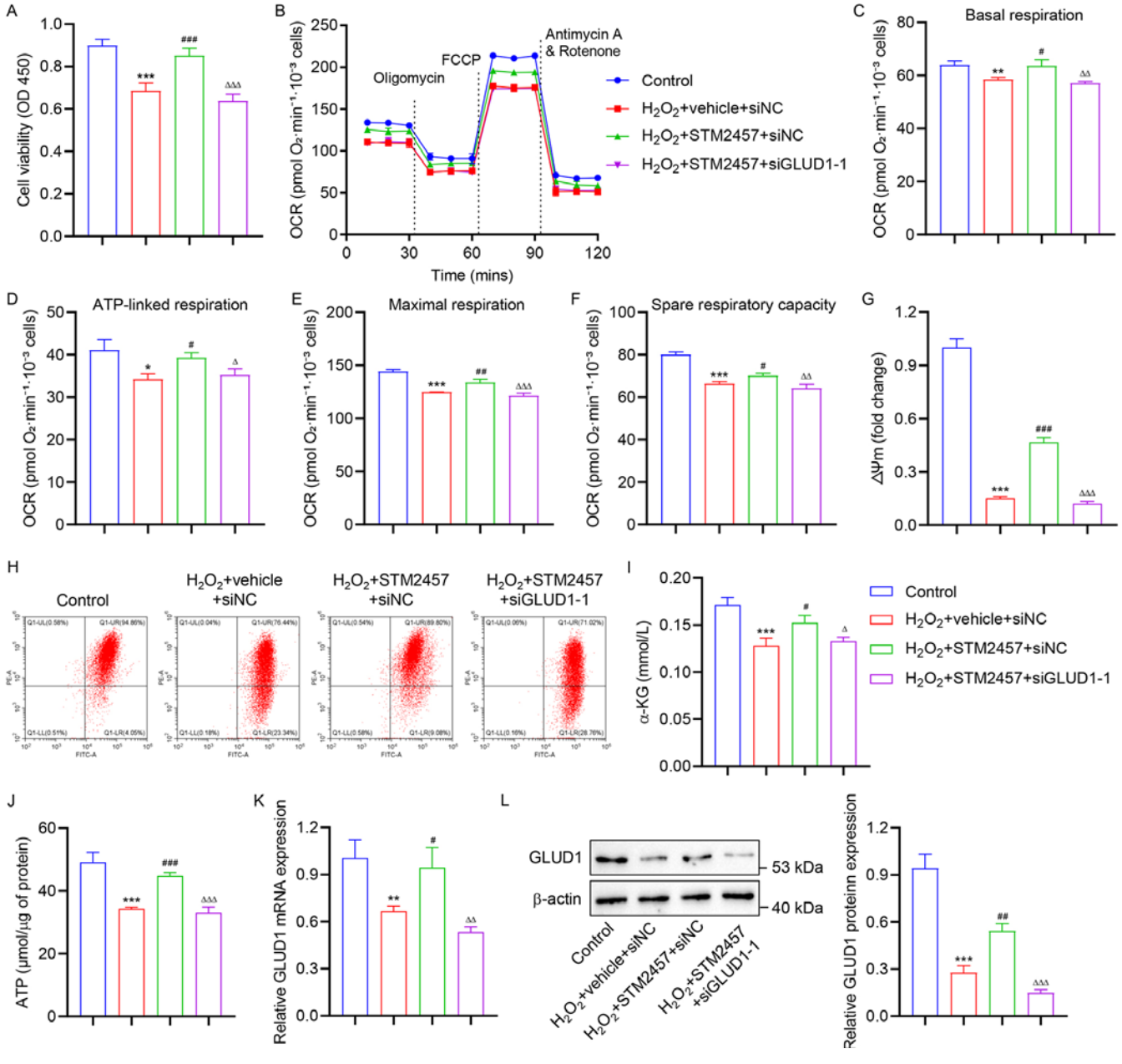

Figure 6. METTL3-induced GLUD1 m6A modification regulates H_2O_2-induced oxidative phosphorylation, MMP, and α-KG production in HNPCs. GLUD1 siRNA pre-transfected HNPCs cells for 24 h, and then treated with H_2O_2 (100 μM) alone or in combination with 5 μM METTL3 inhibitor STM2457 or DMSO vehicle for 24 h. All groups were DMSO-matched to 0.01% (v/v). (A) Cell viability was detected by CCK8. (B-F) OCR was detected by XFe96 Extracellular Flux Analyzer. OCR reported as pmol $O_2 \cdot min^{-1} \cdot 10^{-3}$ cells (normalized to cell number). (G, H) MMP was detected by flow cytometry, and biochemical detection was performed for (I) α-KG and (J) ATP content. GLUD1 expression was detected by (K) qRT-PCR and (L) Western blot. Data are mean ± SD (n = 3 biological replicates). One-way ANOVA followed by Tukey's post hoc test was used. *p<0.05, **p<0.01, ***p<0.001 vs control. $^{\#}p$<0.05, $^{\#\#}p$<0.01, $^{\#\#\#}p$<0.001 vs H_2O_2+vehicle+siNC. $^{\Delta}p$<0.05, $^{\Delta\Delta}p$<0.01, $^{\Delta\Delta\Delta}p$<0.001 vs H_2O_2+STM2457+siNC.

reversing the STM2457-induced increases (Figure 6B–H). STM2457 likewise increased α-KG and ATP levels, while GLUD1 knockdown decreased STM2457-induced α-KG and ATP (Figure 6I,J). Consistent with these functional effects, METTL3 inhibition upregulated GLUD1 in HNPCs, and GLUD1 knockdown abrogated this increase (Figure 6K,L). These data support a model in which METTL3 regulates GLUD1 via m6A to modulate H_2O_2-induced mitochondrial dysfunction.

Discussion

IVDD is a multifactorial disease involving complex signaling networks and diverse effector molecules[31]. Oxidative stress in HNPCs is a major contributor to IVDD[10]. During oxidative stress, mitochondria generate large amounts of ROS. In HNPCs, ROS act as key mediators of signal transduction, regulating matrix metabolism, pro-inflammatory responses, apoptotic cell death, autophagy, and senescence[12]. Oxidative stress not only accelerates peripheral matrix degradation and inflammation but also reduces cell number and impairs cellular function within the HNPC microenvironment[13]. Accumulation of oxidative products in HNPC tissues establishes a sustained oxidative microenvironment that promotes IVDD progression[31]. Interventions that mitigate oxidative stress can help prevent or delay IVDD[13]; thus, targeting oxidative stress represents a potential therapeutic strategy.

H_2O_2 is widely used *in vitro* to induce oxidative stress[32]. In this study, treating HNPCs with increasing concentrations of H_2O_2 produced mitochondrial damage. GLUD1 knockdown exacerbated H_2O_2-induced mitochondrial dysfunction, whereas GLUD1 overexpression alleviated it. These findings suggest that targeting GLUD1 may counter intracellular oxidative stress.

As the center of cellular energy metabolism, mitochondria regulate cell function and survival[33]. Mitochondrial dysfunction is closely associated with the progression of IVDD[34]. Disruption of MMP further impairs proliferation, induces apoptosis, and aggravates IVDD[35]. In addition, elevated ROS progressively deteriorate mitochondrial function, triggering excessive catabolism in HNPCs and increasing inflammation within the IVDD microenvironment[9]. Oxidative stress–induced mitochondrial dysfunction is implicated in the pathogenesis of IVDD[36]. Restoring mitochondrial function may counteract oxidative stress and subsequent cell death, thereby improving IVDD[14]. In this study, we assessed mitochondrial function by measuring OCR and MMP. GLUD1 knockdown reduced both OCR and MMP, whereas GLUD1 overexpression increased them, mitigating the decreases caused by H_2O_2. Thus, GLUD1 may be an emerging regulator of mitochondrial function and a potential modifier of IVDD progression.

α-KG participates in diverse metabolic processes, including the biosynthesis of amino acids, nucleotides, lipids, and carnitines, and it serves as a cofactor for multiple dioxygenases[37]. It also contributes to mitochondrial metabolic homeostasis, collagen synthesis, antioxidant defense, anti-inflammatory responses, cell proliferation, epigenetic modification, and tumor suppression[38]. Although many studies of α-KG have focused on tumor cells—where energy production involves not only glycolysis but also glutamine metabolism, paralleling aspects of IVDD biology[24]—α-KG has also shown potential to ameliorate osteoarthritis[38]. Here, we first quantified α-KG in HNPCs and found that H_2O_2 decreased α-KG levels. Moreover, modulating GLUD1 produced corresponding changes in α-KG.

RNA m6A methylation participates in multiple aspects of RNA metabolism, including regulation of RNA stability, localization, transport, splicing, and translation[39]. The widespread nature of m6A modifications underlies their involvement in diverse physiological and pathological processes[40]. METTL3 is the most common and widely studied m6A methyltransferase and can regulate protein expression of m6A-modified mRNA subsets[40,41]. In this study, we identified METTL3-induced GLUD1 m6A modifications in HNPCs. As the most prevalent post-transcriptional modification in eukaryotes, m6A has been shown to affect RNA stability[42]. Here, we found that METTL3-mediated m6A methylation of GLUD1 mRNA is recognized by YTHDF2 and may modulate H_2O_2-induced mitochondrial dysfunction via the glutamate/α-KG metabolic axis.

This study has several limitations. First, because the work was performed on commercial HNPCs, generalizability to human patients requires validation in primary HNPCs from individuals with IVDD and in preclinical models. Second, *in vitro* experiments cannot fully recapitulate the complex IVD microenvironment, which is characterized by low glucose, hypoxia, acidic pH, and oxidative stress. Consequently, mitochondrial dysfunction induced *in vitro* may differ from that occurring within the disc *in vivo*. These aspects remain to be clarified in future research.

Conclusions

In summary, this study identifies GLUD1 as a potential therapeutic target for IVDD. GLUD1 protects HNPCs from H_2O_2-induced mitochondrial dysfunction through the glutamate/α-KG metabolic axis. METTL3 regulates GLUD1 expression by installing GLUD1 m6A modifications recognized by YTHDF2. Treatment with STM2457, a METTL3 inhibitor, effectively improved mitochondrial dysfunction. These findings enhance our understanding of the METTL3–GLUD1 regulatory axis and its potential therapeutic relevance in IVDD.

Ethics approval

This study used a commercially available human nucleus pulposus cell line (HUM-iCell-sO12; iCell Bioscience, Shanghai, China). No human participants, primary human specimens, or identifiable private information were involved; therefore, institutional ethics approval and informed consent were not required.

Authors' contributions

MB conceived and designed the study and drafted the manuscript. YW, YZ, and HZ collected, analyzed, and interpreted the data. PW and SL revised the manuscript for important intellectual content. All authors read and approved the final version of the manuscript.

Funding

This study was supported by the Program for Young Talents of Science and Technology in Universities of the Inner Mongolia Autonomous Region (NJYT23070).

References

1. Vergroesen PP, Kingma I, Emanuel KS, Hoogendoorn RJ, Welting TJ, van Royen BJ, van Dieën JH, Smit TH. Mechanics and biology in intervertebral disc degeneration: a vicious circle. Osteoarthritis Cartilage. 2015;23(7):1057-1070.
2. Liawrungrueang W, Cholamjiak W, Sarasombath P, Jitpakdee K, Kotheeranurak V. Artificial Intelligence Classification for Detecting and Grading Lumbar Intervertebral Disc Degeneration. Spine Surg Relat Res. 2024;8(6):552-559.
3. Alini M, Diwan AD, Erwin WM, Little CB, Melrose J. An update on animal models of intervertebral disc degeneration and low back pain: Exploring the potential of artificial intelligence to improve research analysis and development of prospective therapeutics. JOR Spine. 2023;6(1):e1230.
4. van Uden S, Silva-Correia J, Oliveira JM, Reis RL. Current strategies for treatment of intervertebral disc degeneration: substitution and regeneration possibilities. Biomater Res. 2017;21(1):22.
5. Chao-Yang G, Peng C, Hai-Hong Z. Roles of NLRP3 inflammasome in intervertebral disc degeneration. Osteoarthritis Cartilage. 2021;29(6):793-801.
6. Lan T, Shiyu-Hu, Shen Z, Yan B, Chen J. New insights into the interplay between miRNAs and autophagy in the aging of intervertebral discs. Ageing Res Rev. 2021;65:101227.
7. Ashley JW, Enomoto-Iwamoto M, Smith LJ, Mauck RL, Chan D, Lee J, Heyworth MF, An H, Zhang Y. Intervertebral disc development and disease-related genetic polymorphisms. Genes Dis. 2016;3(3):171-177.
8. Zhao Y, Qiu C, Wang W, Peng J, Cheng X, Shangguan Y, Xu M, Li J, Qu R, Chen X, Jia S, Luo D, Liu L, Li P, Guo F, Vasilev K, Liu L, Hayball J, Dong S, Pan X, Li Y, Guo L, Cheng L, Li W. Cortistatin protects against intervertebral disc degeneration through targeting mitochondrial ROS-dependent NLRP3 inflammasome activation. Theranostics. 2020;10(15):7015-7033.
9. Yu H, Hou G, Cao J, Yin Y, Zhao Y, Cheng L. Mangiferin Alleviates Mitochondrial ROS in Nucleus Pulposus Cells and Protects against Intervertebral Disc Degeneration via Suppression of NF-κB Signaling Pathway. Oxid Med Cell Longev. 2021;2021:6632786.
10. Yin H, Wang K, Das A, Li G, Song Y, Luo R, Cheung JPY, Zhang T, Li S, Yang C. The REDD1/TXNIP Complex Accelerates Oxidative Stress-Induced Apoptosis of Nucleus Pulposus Cells through the Mitochondrial Pathway. Oxid Med Cell Longev. 2021;2021:7397516.
11. Kang L, Xiang Q, Zhan S, Song Y, Wang K, Zhao K, Li S, Shao Z, Yang C, Zhang Y. Restoration of Autophagic Flux Rescues Oxidative Damage and Mitochondrial Dysfunction to Protect against Intervertebral Disc Degeneration. Oxid Med Cell Longev. 2019;2019:7810320.
12. Feng C, Yang M, Lan M, Liu C, Zhang Y, Huang B, Liu H, Zhou Y. ROS: Crucial Intermediators in the Pathogenesis of Intervertebral Disc Degeneration. Oxid Med Cell Longev. 2017;2017:5601593.
13. Suzuki S, Fujita N, Hosogane N, Watanabe K, Ishii K, Toyama Y, Takubo K, Horiuchi K, Miyamoto T, Nakamura M, Matsumoto M. Excessive reactive oxygen species are therapeutic targets for intervertebral disc degeneration. Arthritis Res Ther. 2015;17:316.
14. González R, Ferrín G, Hidalgo AB, Ranchal I, López-Cillero P, Santos-Gónzalez M, López-Lluch G, Briceño J, Gómez MA, Poyato A, Villalba JM, Navas P, de la Mata M, Muntané J. N-acetylcysteine, coenzyme Q10 and superoxide dismutase mimetic prevent mitochondrial cell dysfunction and cell death induced by d-galactosamine in primary culture of human hepatocytes. Chem Biol Interact. 2009;181(1):95-106.
15. Albaradei S, Thafar M, Alsaedi A, Van Neste C, Gojobori T, Essack M, Gao X. Machine learning and deep learning methods that use omics data for metastasis prediction. Comput Struct Biotechnol J. 2021;19:5008-5018.
16. Tan J, Shi M, Li B, Liu Y, Luo S, Cheng X. Role of arachidonic acid metabolism in intervertebral disc degeneration: identification of potential biomarkers and therapeutic targets via multi-omics analysis and artificial intelligence strategies. Lipids Health Dis. 2023;22(1):204.
17. Lander SS, Chornyy S, Safory H, Gross A, Wolosker H, Gaisler-Salomon I. Glutamate dehydrogenase deficiency disrupts glutamate homeostasis in hippocampus and prefrontal cortex and impairs recognition memory. Genes Brain Behav. 2020;19(6):e12636.
18. Marsico M, Santarsiero A, Pappalardo I, Convertini P, Chiummiento L, Sardone A, Di Noia MA, Infantino V, Todisco S. Mitochondria-Mediated Apoptosis of HCC Cells Triggered by Knockdown of Glutamate Dehydrogenase 1: Perspective for Its Inhibition through Quercetin and Permethylated Anigopreissin A. Biomedicines. 2021;9(11):1664.
19. Zhang J, Wang G, Mao Q, Li S, Xiong W, Lin Y, Ge J. Glutamate dehydrogenase (GDH) regulates bioenergetics and redox homeostasis in human glioma. Oncotarget. 2016
20. Missailidis D, Sanislav O, Allan CY, Smith PK, Annesley SJ, Fisher PR. Dysregulated Provision of Oxidisable Substrates to the Mitochondria in ME/CFS Lymphoblasts. Int J Mol Sci. 2021;22(4):2046.
21. Wu N, Yang M, Gaur U, Xu H, Yao Y, Li D. Alpha-Ketoglutarate: Physiological Functions and Applications. Biomol Ther. 2016;24(1):1-8.
22. Mastorodemos V, Zaganas I, Spanaki C, Bessa M,

Plaitakis A. Molecular basis of human glutamate dehydrogenase regulation under changing energy demands. J Neurosci Res. 2005;79(1-2):65-73.
23. Nakamoto C, Kawamura M, Nakatsukasa E, Natsume R, Takao K, Watanabe M, Abe M, Takeuchi T, Sakimura K. GluD1 knockout mice with a pure C57BL/6N background show impaired fear memory, social interaction, and enhanced depressive-like behavior. PLoS One. 2020;15(2):e0229288.
24. Jin L, Li D, Alesi GN, Fan J, Kang HB, Lu Z, Boggon TJ, Jin P, Yi H, Wright ER, Duong D, Seyfried NT, Egnatchik R, DeBerardinis RJ, Magliocca KR, He C, Arellano ML, Khoury HJ, Shin DM, Khuri FR, Kang S. Glutamate Dehydrogenase 1 Signals through Antioxidant Glutathione Peroxidase 1 to Regulate Redox Homeostasis and Tumor Growth. Cancer Cell. 2015;27(2):257-270.
25. Zhao BS, Roundtree IA, He C. Post-transcriptional gene regulation by mRNA modifications. Nat Rev Mol Cell Biol. 2017;18(1):31-42.
26. Li G, Ma L, He S, Luo R, Wang B, Zhang W, Song Y, Liao Z, Ke W, Xiang Q, Feng X, Wu X, Zhang Y, Wang K, Yang C. WTAP-mediated m6A modification of lncRNA NORAD promotes intervertebral disc degeneration. Nat Commun. 2022;13(1):1469.
27. Han J, Kong H, Wang X, Zhang XA. Novel insights into the interaction between N6-methyladenosine methylation and noncoding RNAs in musculoskeletal disorders. Cell Prolif. 2022;55(10):e13294.
28. Li G, Luo R, Zhang W, He S, Wang B, Liang H, Song Y, Ke W, Shi Y, Feng X, Zhao K, Wu X, Zhang Y, Wang K, Yang C. m6A hypomethylation of DNMT3B regulated by ALKBH5 promotes intervertebral disc degeneration via E4F1 deficiency. Clin Transl Med. 2022;12(3):e765.
29. Chen X, Wang J, Tahir M, Zhang F, Ran Y, Liu Z, Wang J. Current insights into the implications of m6A RNA methylation and autophagy interaction in human diseases. Cell Biosci. 2021;11(1):147.
30. Li F, Zhao D, Wu J, Shi Y. Structure of the YTH domain of human YTHDF2 in complex with an m6A mononucleotide reveals an aromatic cage for m6A recognition. Cell Res. 2014;24(12):1490-1492.
31. Wang Y, Zuo R, Wang Z, Luo L, Zhou Y. Kinsenoside ameliorates intervertebral disc degeneration through the activation of AKT-ERK1/2-Nrf2 signaling pathway. Aging. 2019;11(18):7961-7977.
32. Chen H, Huang X, Fu C, Wu X, Peng Y, Lin X, Wang Y. Recombinant Klotho Protects Human Periodontal Ligament Stem Cells by Regulating Mitochondrial Function and the Antioxidant System during H_2O_2-Induced Oxidative Stress. Oxid Med Cell Longev. 2019;2019:9261565.
33. Abate M, Festa A, Falco M, Lombardi A, Luce A, Grimaldi A, Zappavigna S, Sperlongano P, Irace C, Caraglia M, Misso G. Mitochondria as playmakers of apoptosis, autophagy and senescence. Semin Cell Dev Biol. 2020;98:139-153.
34. Song Y, Li S, Geng W, Luo R, Liu W, Tu J, Wang K, Kang L, Yin H, Wu X, Gao Y, Zhang Y, Yang C. Sirtuin 3-dependent mitochondrial redox homeostasis protects against AGEs-induced intervertebral disc degeneration. Redox Biol. 2018;19:339-353.
35. Saberi M, Zhang X, Mobasheri A. Targeting mitochondrial dysfunction with small molecules in intervertebral disc aging and degeneration. GeroScience. 2021;43(2):517-537.
36. Song D, Ge J, Wang Y, Yan Q, Wu C, Yu H, Yang M, Yang H, Zou J. Tea Polyphenol Attenuates Oxidative Stress-Induced Degeneration of Intervertebral Discs by Regulating the Keap1/Nrf2/ARE Pathway. Oxid Med Cell Longev. 2021;2021:6684147.
37. Yang L, Venneti S, Nagrath D. Glutaminolysis: A Hallmark of Cancer Metabolism. Annu Rev Biomed Eng. 2017;19(1):163-194.
38. Liu L, Zhang W, Liu T, Tan Y, Chen C, Zhao J, Geng H, Ma C. The physiological metabolite α-ketoglutarate ameliorates osteoarthritis by regulating mitophagy and oxidative stress. Redox Biol. 2023;62:102663.
39. Chen XY, Zhang J, Zhu JS. The role of m6A RNA methylation in human cancer. Mol Cancer. 2019;18(1):103.
40. Chen JX, Chen DM, Wang D, Xiao Y, Zhu S, Xu XL. METTL3/YTHDF2 m6A axis promotes the malignant progression of bladder cancer by epigenetically suppressing RRAS. Oncol Rep. 2023;49(5):94.
41. Lin S, Choe J, Du P, Triboulet R, Gregory Richard I. The m(6)A Methyltransferase METTL3 Promotes Translation in Human Cancer Cells. Molecular Cell. 2016;62(3):335-345.
42. Zhu Y, Peng X, Zhou Q, Tan L, Zhang C, Lin S, Long M. METTL3-mediated m6A modification of STEAP2 mRNA inhibits papillary thyroid cancer progress by blocking the Hedgehog signaling pathway and epithelial-to-mesenchymal transition. Cell Death Dis. 2022;13(4):358.

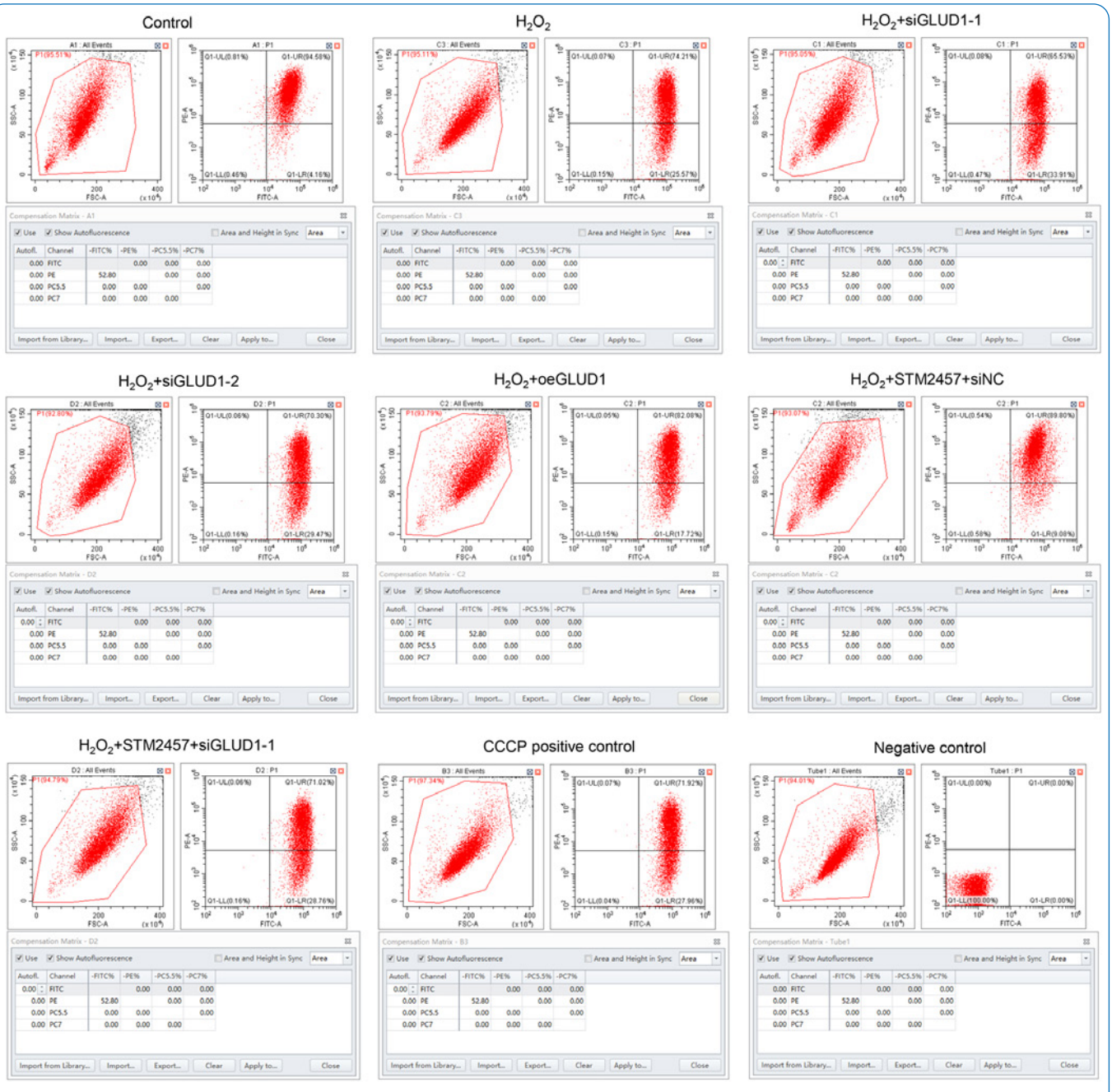

Supplementary Figure S1. Representative flow cytometry plots (gating strategy, compensation, positive/negative controls) for JC-1.

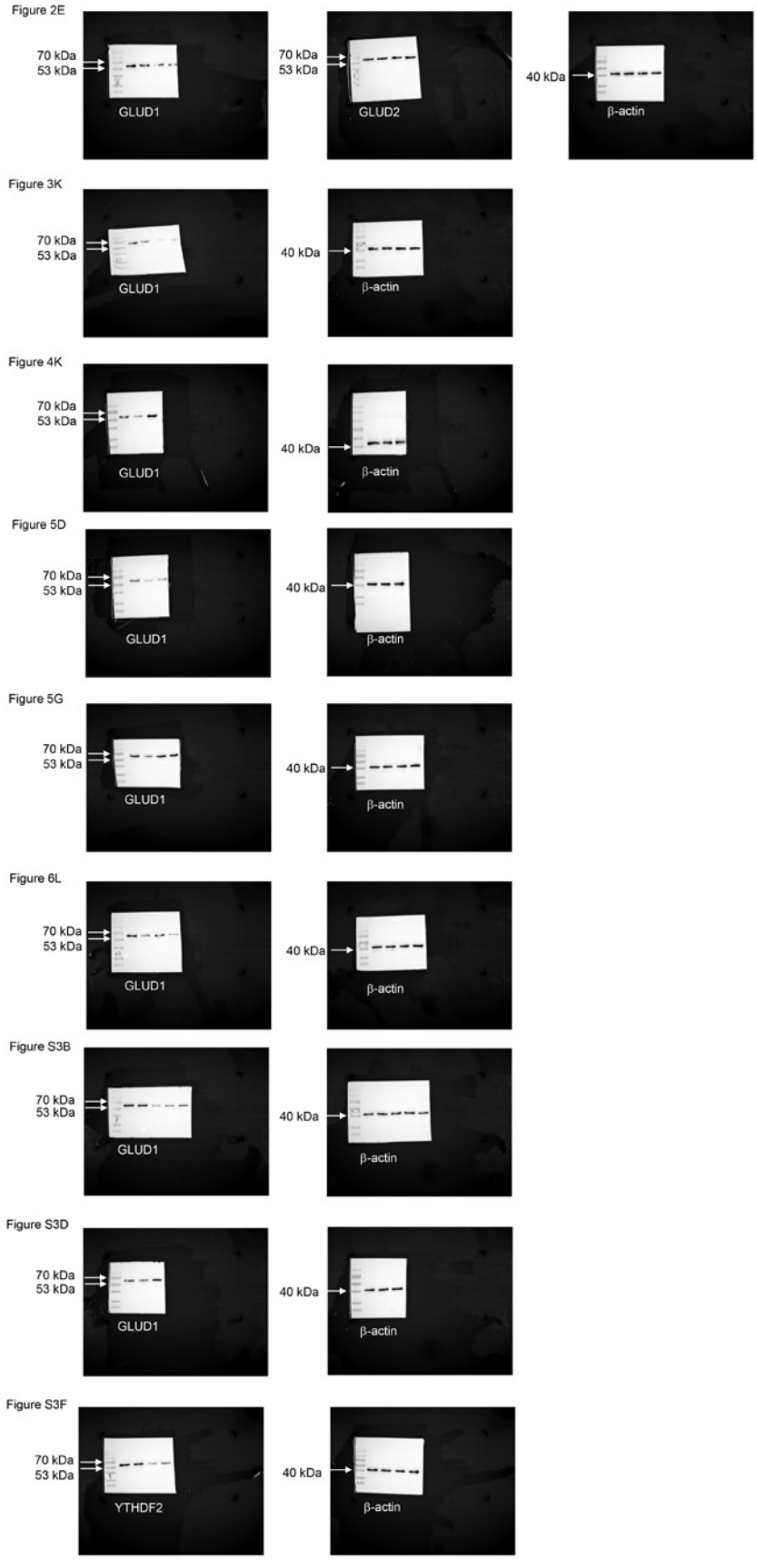

Supplementary Figure S2. Uncropped Western blots with molecular weight markers for all quantified bands.

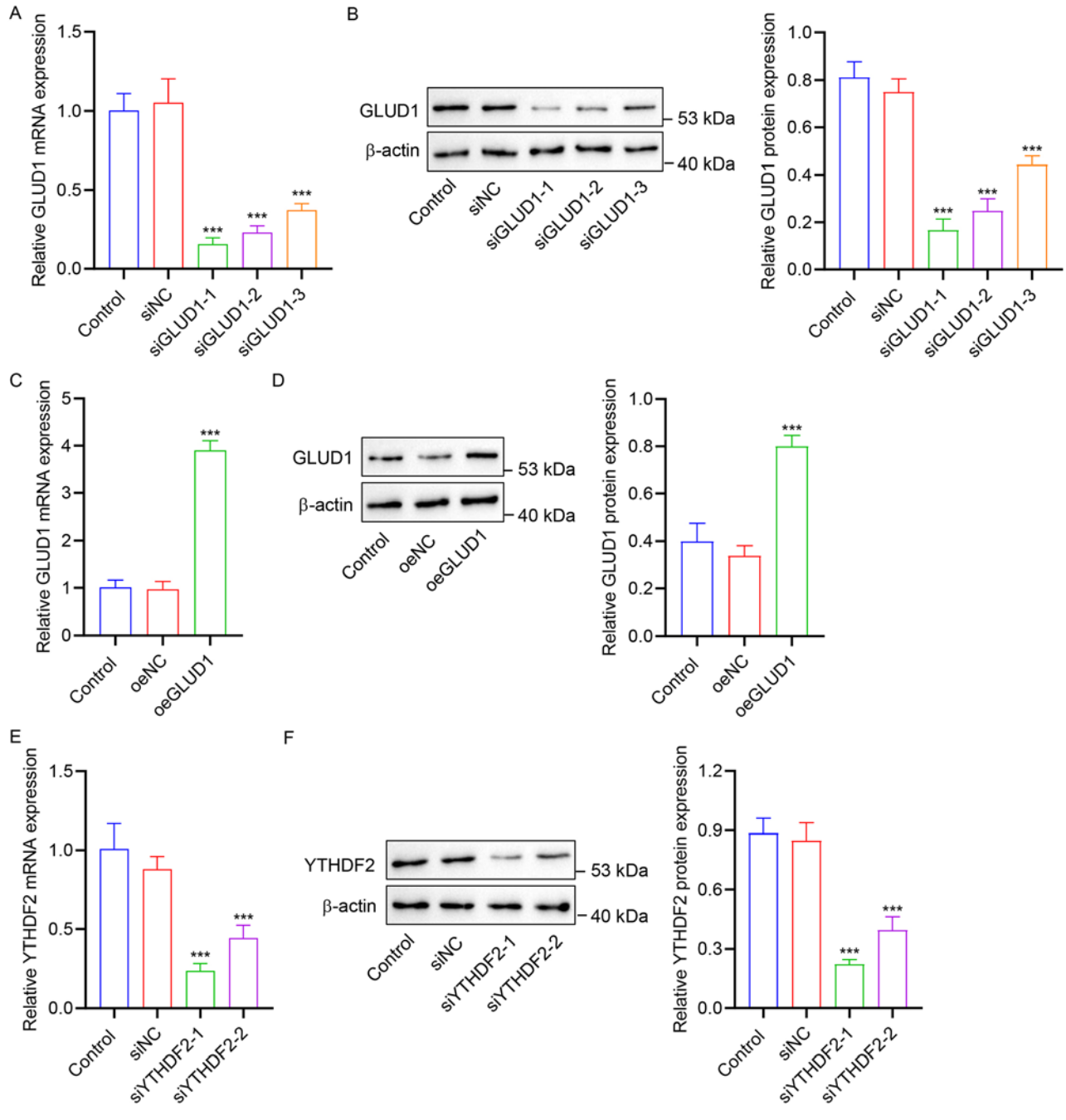

Supplementary Figure S3. GLUD1 and YTHDF2 knockdown or overexpression in HNPCs. GLUD1 siRNA or overexpressed vector was transfected into HNPCs, and GLUD1 expression was detected by (A, C) qRT-PCR and (B, D) Western blot. HNPCs cells were transfected with YTHDF2 siRNA, and the expression of YTHDF2 was detected by (E) qRT-PCR and (F) Western blot. The results are presented as mean ± SD (n=3). All experiments were repeated three times. One-way ANOVA followed by Tukey's post-hoc test was used. ***p<O.OO1 vs siNC or oeNC.